EARTHQUAKE ENGINEERING AND STRUCTURAL DYNAMICS, VOL. 26, 1259–1281 (1997)

A BAYESIAN PROBABILISTIC APPROACH FOR STRUCTURE DAMAGE DETECTION

HOON SOHN*† AND KINCHO H. LAW‡
Department of Civil Engineering, Standford University, Stanford, CA 94305-4020, U.S.A.

SUMMARY

A Bayesian probabilistic approach is presented for the damage detection of multistorey frame structures. In this paper, a Bayesian probabilistic approach is applied to identify multiple damage locations using estimated modal parameters when (1) the measurement data are potentially corrupted with noise, (2) only a small number of degrees of freedom are measured, and (3) a few fundamental modes are estimated. To reduce the potentially intensive computational cost of the proposed method, a branch-and-bound search scheme is proposed and a simplified approach for the modelling of multistorey frame structures is employed. A six-storey shear frame example and two multistorey frame examples, with multiple damage locations, are presented to illustrate the applicability of the proposed approach. © 1997 John Wiley & Sons, Ltd.

Earthquake Engng. Struct. Dyn., **26**, 1259–1281 (1997)

No. of Figures: 7. No. of Tables: 12. No. of References: 25.

KEY WORDS: damage detection; Bayesian probabilistic approach; branch-and-bound search; modal parameters; multistorey frame structures

1. INTRODUCTION

The ability to monitor the health of building structures is an important activity for the maintenance of a facility. With recent advances in damage detection, the monitoring of a structure is within the capability of current technology. Damage detection methods can be classified into *model-based* and *non-model-based* methods.[1] Model-based damage detection methods locate and quantify damage by correlating an analytical model with test data of the damaged structure. Non-model-based methods assess damage by comparing measurements from the undamaged and damaged structures. Model-based methods can provide quantitative information of damage as well as damage locations. However, these methods are computationally intensive and require a Finite Element (FE) model, which is carefully refined with test data of the undamaged structure. While non-model-based methods are simple and straightforward, these methods generally do not provide quantitative information about structural damage. The proposed method is a model-based method and uses modal vibration test data to characterize the state of the structure. Typically, the procedure for model-based damage detection includes four basic steps:

1. *Model construction*: construct an analytical model and identify structural parameters which closely represent the structure.

* Correspondence to: Kincho H. Law, Department of Civil Engineering, Stanford University, Stanford, CA 94305-4020, U.S.A. E-mail: law@ce.stanford.edu
† Graduate Student
‡ Professor

Contract grant sponsor: National Science Foundation; Contract grant number: CMS-95261-2

CCC 0098–8847/97/121259–23$17·50

Received 5 November 1996
Revised 1 May 1997

2. *Modal testing*: estimate modal parameters, i.e. the natural frequencies and the modal vectors, corresponding to the current state of the structure.
3. *Damage localization*: locate the most likely damaged regions using the estimated modal parameters.
4. *Damage assessment and system updating*: assess the severity of damage and update the system parameters.

Model updating and parameter estimation techniques have been developed to improve the analytical model using estimated modal data.[2–4] For damage detection, the analytical model refined by the parameter estimating techniques can be employed as the initial model of the undamaged structure. However, differences between the actual response of the structure and the theoretical response of the analytical model are unavoidable even after the refinement. The differences arise mainly from two types of uncertainties. The first type of uncertainty is due to the presence of noise in the measurements during vibration tests. The second type of uncertainty is the modelling error which arises from the assumptions and simplifications made during the modelling process.[5] Many damage detection methods assume that the initial analytical model is identical to the structure before any damage occurrence.[6–11] The framework of the proposed method explicitly takes into account the modelling error as well as the measurement noise.

There are two common modal testing procedures, ambient and forced vibration tests. A thorough comparison of ambient and forced vibration tests can be found in Reference 12. Ambient vibration tests measure dynamic responses during the normal operation of a structure, and can be easily repeated to collect modal data sets. One difficulty with ambient tests is that the conventional frequency-response function analysis techniques may not be employed because the forcing function is often unknown. Recently, developed system identification techniques are able to estimate modal parameters from ambient vibration tests.[12,13] Forced vibration tests are performed by imposing a known excitation on the structure. Forced vibration tests are generally performed under closely controlled conditions and, consequently, provide more informative data than those obtained by ambient tests. The time and effort required for forced vibration tests are, however, much greater than those for ambient tests. This study focuses on the development of a damage detection method that can be employed in conjunction with an on-line monitoring system.[14] Since an automated monitoring system for a large civil structure will most likely to use ambient excitation, we assume that the experimental modal data can be accumulated by ambient vibration tests. To best utilize the accumulated data, we employ a Bayesian probabilistic approach as a heuristic means to combine previous experimental data with newly available test data. Bayesian probabilistic approaches have been applied to damage detection problems by previous researchers.[8,15,16] To reduce the potentially intensive computational cost of a Bayesian approach, this paper employs a branch-and-bound search scheme and a simplified approach for the modelling of multistorey frame structures.

For damage localization and assessment, residual force vectors (also known as damage vectors or dynamic residual forces) have been employed to locate the most likely damaged regions which are mathematically expressed in terms of degrees of freedom (DOFs) in the analytical model.[6,10,17] For the calculation of residual force vectors, the DOFs in the analytical model should coincide with those in the estimated modal vectors. When only a small number of sensors are installed, one can use either system condensation techniques or modal expansion techniques. System condensation techniques reduce the DOFs defined in the analytical model to the measured DOFs. Reduction techniques often produce a condensed matrix that does not resemble the member connectivity of the original model. As a result, locating damaged members from the residual force vectors of the reduced system becomes very difficult.[18,19] An alternative is to expand the modal vectors, based on the measurements at the instrumented DOFs, to the size of the analytical model.[20,21] Modal expansion methods generally do not produce the results that are accurate enough to provide reliable information about damaged DOFs or damaged structural members.

Instead of employing residual force vectors, we search for the most probable damage locations by comparing the relative probabilities for different damage events. The relative probability of a damage event is expressed in terms of the posterior probability of the damage event, given the estimated modal data sets from the structure. In the proposed method, the formulation of the relative posterior probability is based on the modal output

error, which is defined as the difference between the estimated modal parameters and the theoretical modal parameters from the analytical model. Using an output-error approach, we avoid the aforementioned problems introduced by either modal expansion or reduction techniques.

This paper is organized as follows: The next section describes the theoretical formulation of the Bayesian probabilistic approach. Section 3 presents numerical examples to illustrate the effectiveness of the proposed method. Section 4 summarizes this paper and discusses future work.

2. THEORETICAL FORMULATION

This section presents a damage detection method based on a Bayesian probabilistic approach. First, explicitly considering both modelling and noise errors, we formulate the relative posterior probability of an assumed damage event, which can include multiple substructures as damaged. For the assumed damage locations, the most likely amount of damage is also determined during the calculation of the relative posterior probability. Second, we apply a branch-and-bound search scheme to identify the most likely damage event without searching through all possible damage events. Third, to simplify three-dimensional multistorey frame analyses, a modelling technique based on the rigid-floor diaphragm assumption is employed and extended for damage detection.

2.1. Notations and assumptions

For an analytical model of a structure, we represent the system stiffness matrix $\mathbf{K}$ as an assembly of substructure stiffness matrices. For a model with N_{sub} substructures, the overall stiffness matrix can be expressed as

$$\mathbf{K}(\Theta) = \sum_{i=1}^{N_{\text{sub}}} \theta_i \mathbf{K}_{si} \tag{1}$$

where $\mathbf{K}_{si}$ is the stiffness matrix of the ith substructure and θ_i $(0 \leqslant \theta_i \leqslant 1)$ is a non-dimensional parameter which represents the contribution of the ith substructure stiffness to the system stiffness matrix. The non-dimensional parameter θ_i is introduced to allow the modelling of damage in the ith substructure. A substructure is said to have damaged when the θ value is less than a specified threshold. As damage locations and amount are determined according to the θ values, the system stiffness matrix in equation (1) is expressed as a function of $\Theta = \{\theta_i;\ i = 1, \ldots, N_{\text{sub}}\}$.

Modal data sets are assumed to be collected and estimated from repeated or continuous vibration tests. When vibration tests are repeated N_{s} times, the total collection of N_{s} modal data sets is denoted as

$$\hat{\Psi}_{N_{\text{s}}} = \{\hat{\psi}(n):\ n = 1, \ldots, N_{\text{s}}\} \tag{2}$$

A modal data set $\hat{\psi}(n)$ in equation (2) consists of both the frequencies and the modal vectors estimated from the nth vibration test, i.e.,

$$\hat{\psi}(n) = [\hat{\omega}_1^n, \ldots, \hat{\omega}_{N_{\text{m}}}^n, \hat{\mathbf{v}}_1^{n\text{T}}, \ldots, \hat{\mathbf{v}}_{N_{\text{m}}}^{n\text{T}}]^{\text{T}} \in \mathbf{R}^{N_{\text{t}}} \tag{3}$$

where $\hat{\omega}_i^n$ and $\hat{\mathbf{v}}_i^n$, respectively, denote the ith estimated frequency and modal vector in the nth data set. The modal vector $\hat{\mathbf{v}}_i^n$ $(\hat{\mathbf{v}}_i^n \in \mathbf{R}^{N_{\text{d}}})$ has components corresponding to the instrumented DOFs. The variables N_{t}, N_{d} and N_{m} represent the total number of components in a data set $\hat{\psi}(n)$, the number of the measured DOFs and the number of measured modes, respectively.

Let H_j denote a hypothesis for a damage event which can contain any number of substructures as damaged, and the initial degree of belief about the hypothesis H_j is represented with a prior probability $P(\text{H}_j)$. Using Baye's theorem, the posterior probability $P(\text{H}_j|\hat{\Psi}_{N_{\text{s}}})$, after observing a set of estimated modal parameters $\hat{\Psi}_{N_{\text{s}}}$, can be represented as:

$$P(\text{H}_j|\hat{\Psi}_{N_{\text{s}}}) = \frac{P(\hat{\Psi}_{N_{\text{s}}}|\text{H}_j)}{P(\hat{\Psi}_{N_{\text{s}}})} P(\text{H}_j) \tag{4}$$

The most likely damaged substructures are the ones included in the hypothesis H_{max} which has the largest posterior probability, i.e.

$$P(H_{max}|\hat{\Psi}_{N_s}) = \max_{\forall H_j} P(H_j|\hat{\Psi}_{N_s}) \tag{5}$$

Since the objective is to determine the most probable damage hypothesis, the relative posterior probabilities of alternative hypotheses are of interest. We attempt to avoid the explicit expression of a posterior probability $P(H_j|\hat{\Psi}_{N_s})$ and the examination of all hypotheses. The precise calculation of $P(\hat{\Psi}_{N_s}|H_j)$ is a difficult task. Furthermore, the calculation of the denominator $P(\hat{\Psi}_{N_s})$ in equation (4) involves summing $P(\hat{\Psi}_{N_s}|H_j) \cdot P(H_j)$ over every possible hypothesis. The number of all possible damage events (the size of hypothesis space) for a structure with N_{sub} substructures is equal to $2^{N_{sub}}$. For a large structure, the size of the hypothesis space easily becomes intractable and the computational cost is prohibitive. To overcome these difficulties, we focus on the relative comparisons of posterior probabilities, and devise a branch-and-bound method to facilitate the search of the hypothesis space. In addition, a simplified modelling technique is employed for multistorey frame analyses. The following subsections discuss these three issues.

2.2. Determination of the most probable damage event

When applying equation (4) to calculate the posterior probability $P(H_j|\hat{\Psi}_{N_s})$, the only undefined term is $P(\hat{\Psi}_{N_s}|H_j)$. The prior probability of a hypothesis $P(H_j)$ is the prior information given by users and the probability of estimated modal data $P(\hat{\Psi}_{N_s})$ is simply a normalizing constant.

As shown in equation (1), less than a unity value for θ_i reflects the stiffness decrease in the ith substructure. As noted earlier, when θ_i is less than a specified threshold $\theta_i^*(<1)$, the ith substructure is defined as *damaged*. If we define $\Theta_{H_j}^1$ as a set of θ_i's corresponding to the damaged substructures in a hypothesis H_j and $\Theta_{H_j}^2$ as the rest of θ_i's, the conditional probability $P(\hat{\Psi}_{N_s}|H_j)$ can be interpreted as the probability of obtaining $\hat{\Psi}_{N_s}$, when θ_i's in $\Theta_{H_j}^1$ are less than or equal to their threshold θ_i^*'s and the remaining θ_i's stay within $\theta_i^* < \theta_i \leqslant 1$. Denoting $\Omega_{H_j}^*$ as the range of Θ_{H_j} such that $0 \leqslant \Theta_{H_j}^1 \leqslant \Theta_{H_j}^{1,*}$ and $\Theta_{H_j}^{2,*} < \Theta_{H_j}^2 \leqslant 1$, the conditional probability $P(\hat{\Psi}_{H_j}|H_j)$ becomes

$$\begin{aligned} P(\hat{\Psi}_{N_s}|H_j) &= P(\hat{\Psi}_{N_s}|\Theta_{H_j} < \Omega_{H_j}^*) = \frac{P(\hat{\Psi}_{N_s}, \Theta_{H_j} < \Omega_{H_j}^*)}{P(\Theta_{H_j} < \Omega_{H_j}^*)} \\ &= \frac{P(\Theta_{H_j} < \Omega_{H_j}^*|\hat{\Psi}_{N_s})\, P(\hat{\Psi}_{N_s})}{P(\Theta_{H_j} < \Omega_{H_j}^*)} \\ &= \frac{P(\hat{\Psi}_{N_s})}{P(\Theta_{H_j} < \Omega_{H_j}^*)} \int_{\Theta_{H_j} < \Omega_{H_j}^*} f(\Theta_{H_j}|\hat{\Psi}_{N_s})\, d\Theta_{H_j} \end{aligned} \tag{6}$$

where $\Theta_{H_j}^{1,*}$ and $\Theta_{H_j}^{2,*}$ are the sets of damage thresholds for $\Theta_{H_j}^1$ and $\Theta_{H_j}^2$, respectively, and $f(\Theta_{H_j}|\hat{\Psi}_{N_s})$ is a conditional probability density function (PDF) of Θ_{H_j} given $\hat{\Psi}_{N_s}$. Furthermore, $\Theta_{H_j} < \Omega_{H_j}^*$ indicates that Θ_{H_j} are within the range of $\Omega_{H_j}^*$ such that $0 \leqslant \Theta_{H_j}^1 \leqslant \Theta_{H_j}^{1,*}$ and $\Theta_{H_j}^{2,*} < \Theta_{H_j}^2 \leqslant 1$.

If we define the most probable parameter values $\Theta_{H_j}^{max}$, given a hypothesis H_j, such that

$$f(\Theta_{H_j}^{max}|\hat{\Psi}_{N_s}) = \max_{\Theta_{H_j} < \Omega_{H_j}^*} f(\Theta_{H_j}|\hat{\Psi}_{N_s}) \tag{7}$$

then the upper bound of $P(\hat{\Psi}_{N_s}|\mathrm{H}_j)$ in equation (6) becomes

$$P_{\mathrm{U}}(\hat{\Psi}_{N_s}|\mathrm{H}_j) = \frac{P(\hat{\Psi}_{N_s})}{P(\Theta_{\mathrm{H}_j} < \Omega^*_{\mathrm{H}_j})} \int_{\Theta_{\mathrm{H}_j} < \Omega^*_{\mathrm{H}_j}} f(\Theta^{\max}_{\mathrm{H}_j}|\hat{\Psi}_{N_s})\, \mathrm{d}\Theta_{\mathrm{H}_j}$$
$$= \frac{P(\hat{\Psi}_{N_s})}{P(\Theta_{\mathrm{H}_j} < \Omega^*_{\mathrm{H}_j})} f(\Theta^{\max}_{\mathrm{H}_j}|\hat{\Psi}_{N_s}) \int_{\Theta_{\mathrm{H}_j} < \Omega^*_{\mathrm{H}_j}} 1\, \mathrm{d}\Theta_{\mathrm{H}_j} \tag{8}$$

For simplification, we assume if damage occurs, it could have any arbitrary amount with equal probability. That is, we assign a uniform probability density function to θ_i such that

$$f(\theta_i) = \begin{cases} 1 & \text{if } 0 \leqslant \theta_i \leqslant 1 \\ 0 & \text{otherwise} \end{cases} \tag{9}$$

Furthermore, if θ_i's are assumed to be independent, the following two equations hold:

$$f(\Theta_{\mathrm{H}_j}) = \prod_{\forall \theta_i \in \Theta_{\mathrm{H}_j}} f(\theta_i) = 1 \tag{10}$$

$$\frac{1}{P(\Theta_{\mathrm{H}_j} < \Omega^*_{\mathrm{H}_j})} = \frac{1}{\int_{\Theta_{\mathrm{H}_j} < \Omega^*_{\mathrm{H}_j}} f(\Theta_{\mathrm{H}_j})\, \mathrm{d}\Theta_{\mathrm{H}_j}} = \frac{1}{\int_{\Theta_{\mathrm{H}_j} < \Omega^*_{\mathrm{H}_j}} 1\, \mathrm{d}\Theta_{\mathrm{H}_j}} \tag{11}$$

Substituting equation (11) into equation (8), $P_{\mathrm{U}}(\hat{\Psi}_{N_s}|\mathrm{H}_j)$ can be simplified as

$$P_{\mathrm{U}}(\hat{\Psi}_{N_s}|\mathrm{H}_j) = f(\Theta^{\max}_{\mathrm{H}_j}|\hat{\Psi}_{N_s}) P(\hat{\Psi}_{N_s}) \tag{12}$$

The next step is to compute the conditional PDF, $f(\Theta^{\max}_{\mathrm{H}_j}|\hat{\Psi}_{N_s})$. First, let us define a modal error $e(n, \Theta_{\mathrm{H}_j})$ as

$$e(n, \Theta_{\mathrm{H}_j}) = \hat{\psi}(n) - \psi(\Theta_{\mathrm{H}_j}), \quad n = 1, \ldots, N_s \tag{13}$$

where $\hat{\psi}(n)$ is defined in equation (3). Given Θ_{H_j}, an analytical modal data set $\psi(\Theta_{\mathrm{H}_j})$ is defined similar to equation (3) and is obtained by solving an eigenvalue problem, $\mathbf{K}(\Theta_{\mathrm{H}_j})\, \mathbf{v}_i(\Theta_{\mathrm{H}_j}) = \omega_i^2(\Theta_{\mathrm{H}_j}) \mathbf{M}\, \mathbf{v}_i(\Theta_{\mathrm{H}_j})$:

$$\psi(\Theta_{\mathrm{H}_j}) = [\omega_1(\Theta_{\mathrm{H}_j}), \ldots, \omega_{N_m}(\Theta_{\mathrm{H}_j}), \mathbf{v}_1^{\mathrm{T}}(\Theta_{\mathrm{H}_j}), \ldots, \mathbf{v}_{N_m}^{\mathrm{T}}(\Theta_{\mathrm{H}_j})]^{\mathrm{T}} \in \mathbf{R}^{N_t} \tag{14}$$

It should be noted that, for a modal vector $\mathbf{v}_i(\Theta_{\mathrm{H}_j})$ in equation (14), only the components associated with the measured DOFs are included.

The modal error reflects the discrepancy between the measured response of the structure and the response of the associated analytical model. Two types of uncertainties account for this discrepancy. The first type of uncertainty is the measurement uncertainty caused by the presence of noise during vibration tests. The noise specifically accounts for the difference between the unknown true response and the measured response of the structure. The second type of uncertainty arises from the assumptions and simplifications introduced in the modelling process. Thus, the modal error defined in equation (13) can be divided into two parts:

$$e(n, \Theta_{\mathrm{H}_j}) = e_{\mathrm{N}}(n) + e_{\mathrm{M}}(\Theta_{\mathrm{H}_j}) \tag{15}$$

where $e_{\mathrm{N}}(n)$ is the modal error caused by the measurement noise in the nth vibration data set and $e_{\mathrm{M}}(\Theta_{\mathrm{H}_j})$ is the modal error caused by the modelling error. Assuming that each entry or component of $e_{\mathrm{N}}(n)$ is a normal distribution with zero mean, the expectation on both sides of equation (15) with respect to N_s data sets becomes

$$\mathbf{E}[e(n, \Theta_{\mathrm{H}_j})] = \mathbf{E}[e_{\mathrm{N}}(n)] + \mathbf{E}[e_{\mathrm{M}}(\Theta_{\mathrm{H}_j})] = e_{\mathrm{M}}(\Theta_{\mathrm{H}_j}) \tag{16}$$

where $e_M(\Theta_{H_j})$ is assumed to be constant for all N_s data sets. That is, the modelling error is caused only by the inherent difference between the analytical model and the structure regardless of the noise existence.

It appears that $e_M(\Theta_{H_j})$ changes according to the damage locations and amount. However, when damage is not severe, the modelling error can be assumed not to change significantly. In other words, the modal error caused by the modelling error $e_M(\Theta_{H_j})$ can be assumed to be constant and be approximated by $e_M(\Theta_{H_0})$, which is the modal error caused by the modelling error in the healthy (undamaged) state of the structure:

$$e_M(\Theta_{H_j}) \cong e_M(\Theta_{H_0}), \quad \forall \Theta_{H_j} \tag{17}$$

where H_0 is a null hypothesis that there is no damage in the structure and the θ values of the healthy structure are calibrated to have unity values before any damage occurs. From the definition of the modal error and equation (16), $e_M(\Theta_{H_0})$ can be evaluated from the estimated and the analytical modal parameter sets:

$$e_M(\Theta_{H_0}) = \mathbf{E}[e(n, \Theta_{H_0})] = \mathbf{E}[\hat{\psi}^h(n)] - \mathbf{E}[\psi(\Theta_{H_0})] = \hat{\psi}^h_m - \psi(\Theta_{H_0}) \tag{18}$$

where the superscript h denotes the properties of the healthy structure. Since $\psi(\Theta_{H_j})$ is constant with respect to the N_s data sets, $\mathbf{E}[\psi(\Theta_{H_0})] = \psi(\Theta_{H_0})$. Furthermore, the sample mean $\hat{\psi}^h_m$ is used to approximate the expectation $\mathbf{E}[\hat{\psi}^h(n)]$. The ith component of $\hat{\psi}^h_m$ is calculated such that

$$\mathbf{E}[\hat{\psi}^h_i(n)] \cong \hat{\psi}^h_{m,i} = \frac{1}{N^h_s} \sum_{n=1}^{N^h_s} \hat{\psi}^h_i(n) \tag{19}$$

where $i = 1, \ldots, N_t$ and N^h_s is the number of modal data sets before damage occurrence. As a result, $e_M(\Theta_{H_j})$ can be evaluated from the measured modal parameter set $\hat{\psi}^h(n)$ of the healthy structure and the modal parameter set $\psi(\Theta_{H_0})$ of the initial analytical model:

$$e_M(\Theta_{H_j}) \cong e_M(\Theta_{H_0}) = \hat{\psi}^h_m - \psi(\Theta_{H_0}), \quad \forall \Theta_{H_j} \tag{20}$$

From the results of equations (16) and (17), the error $\{e_i(n, \Theta_{H_j}); n = 1, \ldots, N_s\}$ for each component becomes a multivariate normal distribution with mean $e_{M,i}(\Theta_{H_0})$ and variance σ_i. Variance σ_i can be evaluated from the observation of the estimated modal parameter sets. When a large number of experimental data sets are available, sample standard deviations (or variances) can be extracted from the data set. When modal data sets available are not sufficient to estimate the variances, we assign uniform coefficient of variance (COV) to all modal parameters. Assuming that the components of the modal error $e(n, \Theta_{H_j})$ are independent, the conditional joint PDF of Θ_{H_j} becomes

$$f(\Theta_{H_j} | \hat{\Psi}_{N_s}) = f(e(n, \Theta_{H_j}) | \hat{\Psi}_{N_s}) = k \exp\{-J(\hat{\Psi}_{N_s}, \Theta_{H_j})\} \tag{21}$$

where

$$k = \frac{1}{[2\pi]^{N_s/2}} \frac{1}{\|\mathbf{C}_{\hat{\Psi}}\|^{1/2}} \text{ and } \|\mathbf{C}_{\hat{\Psi}}\| = \det|\text{diag}[\sigma_1^2, \ldots, \sigma_{N_t}^2]| = \prod_{i=1}^{N_t} \sigma_i^2.$$

Furthermore, the error function $J(\hat{\Psi}_{N_s}, \Theta_{H_j})$ is

$$J(\hat{\Psi}_{N_s}, \Theta_{H_j}) = \frac{1}{2} \sum_{n=1}^{N_s} [\hat{\psi}(n) - \psi(\Theta_{H_j}) - e_M(\Theta_{H_0})]^T \mathbf{C}^{-1}_{\hat{\Psi}} [\hat{\psi}(n) - \psi(\Theta_{H_j}) - e_M(\Theta_{H_0})] \tag{22}$$

From equations (4), (12) and (21), the upper bound of $P(H_j | \hat{\Psi}_{N_s})$ becomes

$$P_U(H_j | \hat{\Psi}_{N_s}) = f(\Theta^{\max}_{H_j} | \hat{\Psi}_{N_s}) P(H_j) = \exp\{-J(\hat{\Psi}_{N_s}, \Theta^{\max}_{H_j})\} \cdot P(H_j) \cdot k \tag{23}$$

From equation (23) and the fact that the relative comparison of $P_U(H_j|\hat{\Psi}_{N_s})$ is independent of the constant k, the following relationships hold:

$$\begin{aligned}\max[P_U(H_i|\hat{\Psi}_{N_s}), P_U(H_j|\hat{\Psi}_{N_s})] &= \max[\ln P_U(H_i|\hat{\Psi}_{N_s}), \ln P_U(H_j|\hat{\Psi}_{N_s})] \\ &= \min[J(\hat{\Psi}_{N_s}, \Theta_{H_i}^{\max}) - \ln P(H_i), J(\hat{\Psi}_{N_s}, \Theta_{H_j}^{\max}) - \ln P(H_j)] \end{aligned} \tag{24}$$

where ln denotes natural logarithm. Therefore, the most probable hypothesis H_{max} in equation (5) satisfies:

$$J(\hat{\Psi}_{N_s}, \Theta_{H_{max}}^{\max}) - \ln P(H_{max}) = \min_{\forall H_j}[J(\hat{\Psi}_{N_s}, \Theta_{H_j}^{\max}) - \ln P(H_j)] \tag{25}$$

Now, the comparison of posterior probabilities can be conducted by examining only the error function $J(\hat{\Psi}_{N_s}, \Theta_{H_j}^{\max})$ and the prior probability $P(H_j)$. It should be noted that $P_U(H_j|\hat{\Psi}_{N_s})$ is employed rather than $P(H_j|\hat{\Psi}_{N_s})$ in equation (24). The use of $P_U(H_j|\hat{\Psi}_{N_s})$ can be justified as follows: First, assume that H_d and $\Theta_{H_d}^{\max}$ correspond to the actual damage locations and amount. In addition, noise effect is ignored for the current argument. Then, we can expect an inequality $f(\Theta_{H_d}^{\max}|\hat{\Psi}_{N_s}) \geqslant f(\Theta_{H_j}|\hat{\Psi}_{N_s})$ for any H_j and Θ_{H_j}. That is, the conditional PDF of observing H_d and $\Theta_{H_d}^{\max}$ is expected to be higher than or equal to any other damage cases (the equality holds when $H_j = H_d$ and $\Theta_{H_j} = \Theta_{H_d}^{\max}$). From this observation and the fact that $P_U(H_j|\hat{\Psi}_{N_s}) = \int_{\Theta_{H_j} < \Omega_{H_j}^*} f(\Theta_{H_j}^{\max}|\hat{\Psi}_{N_s})\, d\Theta_{H_j}$, $P_U(H_d|\hat{\Psi}_{N_s}) \geqslant P_U(H_j|\hat{\Psi}_{N_s})$ holds for all H_j. However, if Θ_{H_d} differs from $\Theta_{H_d}^{\max}$, the conditional PDF $f(\Theta_{H_d}|\hat{\Psi}_{N_s})$ can be less than other conditional PDFs even though H_d corresponds to the actual damage locations. In other words, the PDF of *correct* damage locations and *incorrect* damage amount can be lower than PDFs of some other damage cases ($f(\Theta_{H_d}|\hat{\Psi}_{N_s}) < f(\Theta_{H_j}|\hat{\Psi}_{N_s})$ for some H_j and Θ_{H_j}). Consequently, $P(H_d|\hat{\Psi}_{N_s})$ can be less than $P(H_j|\hat{\Psi}_{N_s})$ for some H_j. In this case, we may fail to identify the actual damage event. Therefore, the use of $P_U(\hat{\Psi}_{N_s}|H_d)$ appears to increase the chance of identifying the actual damage locations and amount.

For given modal data, while we are interested in the probability $P_U(H_j|\hat{\Psi}_{N_s})$ of the assumed damage locations, the approach in Reference 8 calculates the conditional PDF $f(\Theta|\hat{\Psi}_{N_s})$ where $\Theta = \{\theta_1, \ldots, \theta_{N_{sub}}\}$ and θ_i is defined as a continuous variable with states ranging from 0 to 1. To obtain the probability for some parameter set Θ, a multi-dimensional integration for a desired Θ space is required. This multi-dimensional integral may not be feasible for a large-scale model. This problem can be simplified by assuming that damage is localized in only a single substructure.[8] As an alternative, an asymptotic approach is proposed in Reference 15. However, the asymptotic approach requires the calculation of all the maxima of $f(\Theta|\hat{\Psi}_{N_s})$, which is also a computationally expensive task.

In this study, we define the state of a substructure as *damaged* or *undamaged*. The binary states make it possible to construct a tree representation of all possible damage cases. The *damage tree* starts with a null hypothesis H_0 that no damage is present. From the root, the first level branches are extended by adding a substructure as damaged one at a time. For a system with N_{sub} substructures, the number of the first-level branches becomes ${}_{N_{sub}}C_1$. Here, we define ${}_NC_K (= N!/(K!(N-K)!))$ as the number of combinations of K items out of a population N. From each first-level branch, the second-level branches are extended by adding another substructure as damaged. The total number of the second-level branches becomes ${}_{N_{sub}}C_2$. For a system with N_{sub} substructures, the damage tree has a total N_{sub} levels of branches and the total number of branches is $2^{N_{sub}} = {}_{N_{sub}}C_0 + {}_{N_{sub}}C_1 + \cdots + {}_{N_{sub}}C_{N_{sub}}$. Clearly, the number of alternatives remains large. The complexity can be significantly reduced by a branch-and-bound search scheme, which is originally proposed for the diagnosis of multiple diseases.[22]

2.3. A branch-and-bound search scheme

A branch-and-bound search scheme is proposed to expedite the search for the most likely damage case without exhaustively examining all the possible combinations of damaged substructures. Starting from the null

hypothesis H_0 that no damage is present, one substructure is added as a possible damage location at a time to generate extended hypotheses. The posterior probabilities of hypotheses are examined in terms of their error functions and the prior probabilities as defined in equation (25). Each hypothesis keeps extending by adding a new substructure as damaged until the further addition of substructures does not lead to a more probable hypothesis. The key requirement is a bounding heuristic which allows us to rule out further extensions of a hypothesis. In this study, the following two pruning heuristics are adopted.

1. Let $H_j \cup D_i$ denote an extension of hypothesis H_j by adding the ith substructure as damaged. If a posterior probability of $H_j \cup D_i$ is less than that of H_j, then further extension of $H_j \cup D_i$ is ruled out, i.e.

$$\text{if } P(H_j \cup D_i | \hat{\Psi}_{N_s}) < P(H_j | \hat{\Psi}_{N_s}), \text{ stop extending } H_j \cup D_i. \tag{26}$$

2. If a posterior probability of H_j is less than $P_{\max}$, which is the largest posterior probability among all the hypotheses examined so far, then further extension of H_j is ruled out; i.e.

$$\text{if } P(H_j | \hat{\Psi}_{N_s}) < P_{\max}, \text{ stop extending } H_j \tag{27}$$

Using equation (26), we can exclude the extension of $H_j \cup D_i$ when the addition of the ith substructure as damaged is found not to lead to a more probable hypothesis. In addition, when the first H_j is found such that $P(H_j | \hat{\Psi}_{N_s}) > P(H_j \cup D_i | \hat{\Psi}_{N_s})$ for all substructures not included in H_j ($\forall D_i \notin H_j$), $P(H_j | \hat{\Psi}_{N_s})$ is the first local maximum posterior probability in the current branching direction of damage events. That is, the criterion in equation (26) guarantees that the first local maximum posterior probability in every branching direction is found. Unfortunately, this pruning heuristic is not a strong criterion for the system with a large number of substructures since all branches are subject to further extensions until the first local maximum point is found.

As a complementary criterion, equation (27) excludes the further branching of the newly extended hypotheses which have posterior probabilities less than the largest posterior probability among the hypotheses examined so far. The second criterion can be easily modified to include n number of the newly extended hypotheses for the further branching by replacing $P_{\max}$ in equation (27) with the nth largest posterior probability $P^n_{\max}$. By using the nth largest posterior probability, we can make an explicit trade-off between the better diagnosis and the computational efficiency.

2.4. Modelling of multistorey frame structures

The modelling of a multistorey frame structure can be simplified by assuming that

(1) the floor diaphragm is rigid in its own plane and only flexible in the vertical direction,
(2) the rotational and vertical DOFs can be condensed out of the dynamic analysis, and
(3) the axial deformations of beams and columns are negligible.[23]

The system stiffness matrix of a multistorey frame structure is determined from the lateral stiffness matrices of individual planar frames. The modelling process can be summarized as follows:

1. The stiffness matrix of each planar frame is first computed. Using the same notation as in equation (1), the stiffness matrix of a frame j can be written as

$$\mathbf{K}(\Theta)_j = \sum_{\forall i \in j} \theta_i \mathbf{K}_{si} \tag{28}$$

where the assembly is performed for each substructure i in the jth planar frame ($\forall i \in j$). Neglecting axial deformations in the columns and beams, the model of a planar frame has one in-plane rotational DOF at each node and one lateral DOF at each floor level [see Figure 1(a)].

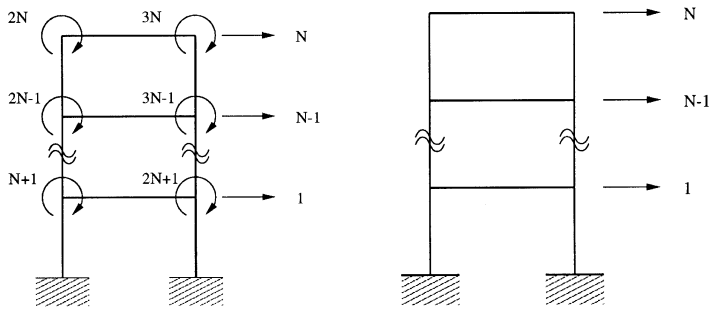

Figure 1. Calculation of lateral stiffness by condensing out rotational DOFs

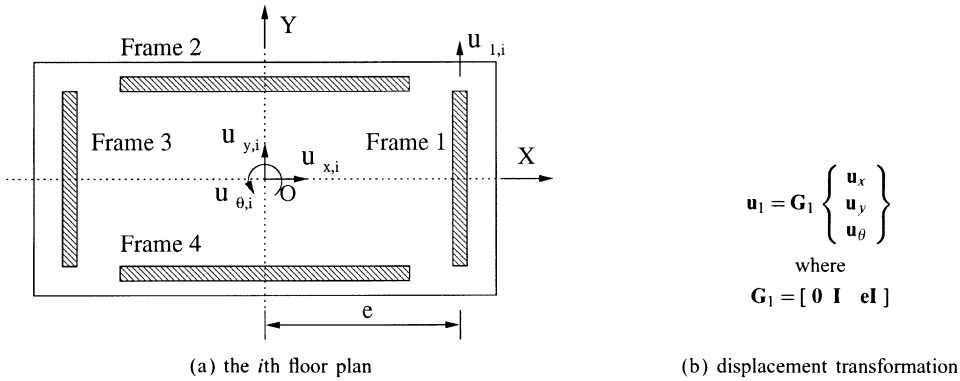

Figure 2. Global DOFs of a system and lateral DOFs of planar frames

2. The lateral stiffness matrix of the individual planar frame is determined from the stiffness matrix of the planar frame. The stiffness matrix of the planar frame can be partitioned according to the lateral (l) and rotational (r) DOFs, respectively,

$$\mathbf{K}(\Theta)_j = \begin{bmatrix} \mathbf{K}_{ll,j} & \mathbf{K}_{lr,j} \\ \mathbf{K}_{rl,j} & \mathbf{K}_{rr,j} \end{bmatrix} \tag{29}$$

Since the inertial effects associated with the rotational DOFs are usually small, the rotational DOFs can be condensed out of the dynamic analysis of the structure [see Figure 1(b)]. Using static condensation, the lateral stiffness of the planar frame $\bar{\mathbf{K}}(\theta)_j$ becomes

$$\bar{\mathbf{K}}(\Theta)_j = \mathbf{P}(\Theta)_j^{\mathrm{T}}\, \mathbf{K}(\Theta)_j\, \mathbf{P}(\Theta)_j \tag{30}$$

where

$$\mathbf{P}(\Theta)_j = \begin{bmatrix} \mathbf{I} \\ -\mathbf{K}_{rr,j}^{-1}\, \mathbf{K}_{rl,j} \end{bmatrix} \tag{31}$$

and $\mathbf{I}$ is an identity matrix. It should be noted that the transformation matrix $\mathbf{P}(\Theta)_j$ is expressed as a function of Θ.

3. Using compatibility conditions, the displacement transformation matrix $\mathbf{G}_j$ can be defined to relate the lateral displacements of the jth frame to the global DOFs of the system

$$\mathbf{u}_j = \mathbf{G}_j \mathbf{u}; \quad j = 1, \ldots, N_{\mathrm{f}} \tag{32}$$

where N_f is the number of planar frames, $\mathbf{u}$ are the global DOFs and $\mathbf{u}_j$ are the lateral DOFs of the jth planar frame. Figure 2(a) shows the global DOFs of the system and the lateral DOFs of planar frames in the ith floor of a multistorey system. An example of the displacement transformation matrix is shown in Figure 2(b).

4. Finally, the system stiffness matrix of the simplified model is obtained by assembling the transformed stiffness matrices of all the planar frames:

$$\mathbf{K}(\Theta) = \sum_{j=1}^{N_f} \mathbf{G}_j^T \tilde{\mathbf{K}}_j \mathbf{G}_j = \sum_{j=1}^{N_f} \mathbf{G}_j^T \mathbf{P}(\Theta)_j^T \mathbf{K}(\Theta)_j \mathbf{P}(\Theta)_j \mathbf{G}_j$$
$$= \sum_{j=1}^{N_f} \mathbf{T}(\Theta)_j^T \mathbf{K}(\Theta)_j \mathbf{T}(\Theta)_j \tag{33}$$

where $\mathbf{T}(\Theta)_j = \mathbf{P}(\Theta)_j \mathbf{G}_j$. After substituting equation (28) into equation (33) and some manipulations, the stiffness matrix of the simplified model can be represented in a similar way to equation (1):

$$\mathbf{K}(\Theta) = \sum_{j=1}^{N_f} \sum_{\forall i \in j} \theta_i \mathbf{T}(\Theta)_j^T \mathbf{K}_{si} \mathbf{T}(\Theta)_j = \sum_{i=1}^{N_{sub}} \theta_i \tilde{\mathbf{K}}(\Theta)_{si} \tag{34}$$

where the effective stiffness contribution of the ith substructure is

$$\tilde{\mathbf{K}}(\Theta)_{si} = \sum_{\forall j \ni i} \mathbf{T}(\Theta)_j^T \mathbf{K}_{si} \mathbf{T}(\Theta)_j \tag{35}$$

To obtain the effective stiffness contribution of the ith substructure, the assembly is performed for all planar frames which include the ith substructure ($\forall j \ni i$). For example, when the ith substructure is common to planar frames 1 and 2, the stiffness contribution of the ith substructure to the system stiffness matrix is $\theta_i(\mathbf{T}(\Theta)_1^T \mathbf{K}_{si} \mathbf{T}(\Theta)_1 + \mathbf{T}(\Theta)_2^T \mathbf{K}_{si} \mathbf{T}(\Theta)_2)$.

This approach neglects compatibility of deformations in columns which are common to more than one frame. The assumption is acceptable except for tall slender buildings or tube-type structures.[24] The system mass matrix is diagonalized by lumping the floor mass and the half-masses of columns connected to the floor. The moment of inertia of the floor diaphragm is calculated about the vertical axis through the centre of mass. Since the damage detection method requires repeated solution of the eigenvalue problem, the computational cost is significantly reduced by using the simplified model.

3. NUMERICAL EXAMPLES

This section presents three examples to illustrate the Bayesian probabilistic approach for the damage detection of frame structures. The example structures include a six-storey shear frame structure, and a two-storey and a five-storey three-dimensional frame structure. For all examples, a uniform prior probability is assigned to all hypotheses. Therefore, the determination of the most probable hypothesis in equation (25) depends only on the error function $J(\hat{\Psi}_{N_s}, \Theta_{H_j}^{max})$. For all numerical examples, the search space $\Theta_{H_j} < \Omega_{H_j}^*$ in equation (7) is evaluated at the intersection of grid lines which discretizes the search domain with an incremental step $\Delta\theta$. For the presented numerical examples, we use an incremental step $\Delta\theta = 0{\cdot}1$. In addition, a value of $0{\cdot}9$ is used for the damage threshold θ^* for every substructure. That is, over 10 per cent decreases in the stiffness are defined as *damage*. Instead of the largest posterior probability P_{max}, we use the third largest posterior probability P_{max}^3 ($< P_{max}^2 < P_{max}^1 = P_{max}$) in equation (27) to investigate a larger subspace of the hypothesis space. The branch-and-bound search in the presented examples follows a depth-first/best-first search strategy. Each modal vector is normalized with respect to the absolute maximum component in the modal vector. Since

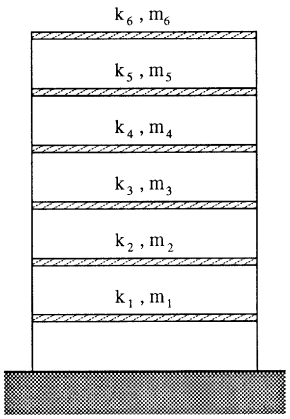

Figure 3. A six-storey shear frame model

one component is used for normalization, only $N_d - 1$ pieces of information exist for each mode. For the examples shown below, L_{dam} and D_{dam} denote the actual damage locations and the associated damage amount, respectively. $\hat{L}_{dam}$ and $\hat{D}_{dam}$ denote the most probable damage locations and the associated damage amount estimated by the proposed method. In addition, the measured DOFs and the estimated modes are denoted by DOFm and MODEm, respectively.

3.1. A six-storey shear frame structure

The first example structure is the six-storey shear frame structure shown in Figure 3. The frame structure consists of six DOFs and six substructures corresponding to each floor storey. To simulate measurement uncertainties in the estimated modal parameters, the exact modal parameters, obtained from the analytical model with the assumed damage, are perturbed with noise. More explicitly, the estimated modal parameter set $\hat{\psi}(n)$ in equation (3) is constructed such that

$$\hat{\psi}(n) = \psi \left(1 + \frac{\mathcal{N}}{100}\,\mathcal{R}\right) \tag{36}$$

where ψ is the exact modal parameter set obtained from the analytical model, $\mathcal{N}$ is a specified noise level in terms of percentage, and $\mathcal{R}$ is a normally distributed random number with zero mean and a variance of 1·0. This process is repeated N_s times to simulate the N_s modal data sets.

Since the estimated modal parameters are simulated by adding noise to the exact modal parameters, the modal error defined in equation (15) arises only from noise error, i.e. $e(n, \Theta_{H_j}) = e_N(n, \Theta_{H_j})$. Therefore, the error function shown in equation (22) is simplified as

$$J(\hat{\Psi}_{N_s}, \Theta_{H_j}) = \frac{1}{2} \sum_{n=1}^{N_s} [\hat{\psi}(n) - \psi(\Theta_{H_j})]^T \mathbf{C}_{\hat{\Psi}}^{-1} [\hat{\psi}(n) - \psi(\Theta_{H_j})] \tag{37}$$

This example investigates the applicability of the proposed method subject to the effects of (1) the noise level in the estimated modal data, (2) the number and the selection of estimated modes and measured DOFs, (3) the locations and the amount of damage, and (4) the number of modal data sets.

3.1.1. Effect of noise level in the estimated modal data. The proposed method is first tested to show that it does not give a false-positive indication of damage (the case of indicating damage when, in fact, damage does not exist). There cases are conducted assuming 3, 5 and 10 per cent noise levels. For each case, 10 sets of modal parameters are simulated from the *undamaged* structure, the DOFs corresponding to the second and

Table I. Effect of noise level

Case	Noise level	Rank
1	0·5%	1
2	1·0%	5
3	5·0%	8
4	10·0%	10

$L_{\text{dam}} = \{2, 6\}$, $D_{\text{dam}} = \{30\%, 10\%\}$, $N_s = 3$, DOFm $= \{2, 4\}$, MODEm $= \{1, 2\}$

Table II. Effect of measured DOFs

Case	DOFm	Rank
1	all	1
2	1, 3, 5	1
3	3, 5	15
4	2, 4	14
5	3	13

$L_{\text{dam}} = \{2, 6\}$, $D_{\text{dam}} = \{30\%, 10\%\}$, $N_s = 5$, MODEm $= \{1, 2\}$, noise $= 10\%$

fourth storeys are measured, and the first and the second modes are identified. For all cases, the proposed method does not provide a false-positive indication.

Next, the effect of noise in the measured data is investigated. Four cases are conducted by varying the noise levels from 0·5 to 10 per cent. For all cases, the stiffnesses of the second and the sixth storeys are decreased by 30 per cent and 10 per cent, respectively, i.e. $L_{\text{dam}} = \{2, 6\}$ and $D_{\text{dam}} = \{30\%, 10\%\}$. The measurements are made at the second and the fourth storeys, and the first and the second modes are identified, i.e. DOFm $= \{2, 4\}$ and MODEm $= \{1, 2\}$. Three sets of modal parameters are collected ($N_s = 3$). Table I summarizes the results. The *rank* in the table indicates the rank of the actual damage event when the posterior probabilities of all examined hypotheses are sorted in descending order. As the noise level increases from case 1 to cases 2, 3 and 4, the rank of the actual damage event decreases.

3.1.2. Effect of measured DOFs. The effect of measured DOFs is examined by changing the number and locations of the measured DOFs. Five cases are conducted by assuming $L_{\text{dam}} = \{2, 6\}$, $D_{\text{dam}} = \{30\%, 10\%\}$, $N_s = 5$ and a 10 per cent noise level for the estimated modal parameters. Table II shows the results. When the modal vectors are obtained from the measurements on all DOFs (case 1) or on alternative floors (case 2), the proposed method correctly identifies the damage locations even in the presence of a 10 per cent noise. As the number of measured DOFs decreases to two or one (cases 3, 4 and 5), the proposed method fails to rank the actual damage event as the most likely one. In case 5 of Table II (where only one DOF is measured), the proposed method uses only the estimated frequency information. No information is provided from modal vectors since the normalization of modal vectors requires the measurements of more than two DOFs. If a larger number of modal data sets were available, the diagnosis result could be improved. This is true even for the cases where only a limited number of locations are measured, and the data have relatively high noise level (see Section 3.1.6).

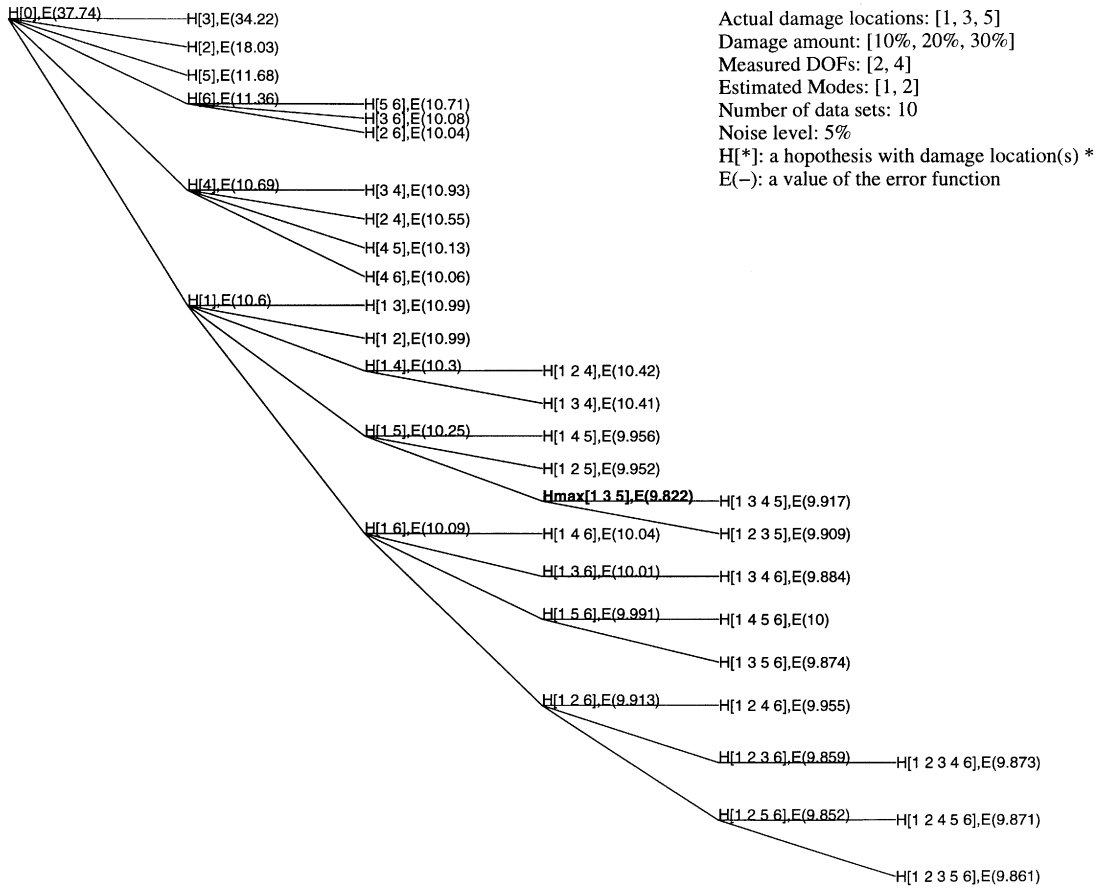

Figure 4. A Branch-and-bound search for damage locations of a six-storey shear frame structure

3.1.3. Effect of multiple damage locations. One salient feature of this work is that multiple damage locations in a structure can be detected. As noted earlier, a branch-and-bound search scheme is employed to facilitate the search of multiple damage locations. Figure 4 presents a typical result of the branch-and-bound search. In this figure, 10, 20 and 30 per cent damages are assumed in the first, the third and the fifth storeys, respectively ($L_{\text{dam}} = \{1, 3, 5\}$ and $D_{\text{dam}} = \{10\%, 20\%, 30\%\}$). The first two modes are estimated by the measurements on the second and the fourth storeys (DOFm = [2, 4] and MODEm = [1, 2]). In addition, 10 modal data sets are simulated by assuming a 5 per cent noise level ($N_s = 10$ and Noise = 5%).

Figure 4 shows that the proposed method finds the actual damage locations after searching 39 hypotheses out of the 64 possible hypotheses. The first storey is detected as damaged immediately in the first step of branching. Since the decrease of the first storey stiffness has a significant effect on all modal parameters, the first storey is easily detected as a damaged substructure. In the next step, the fifth storey, which has the largest damage amount, is detected. Finally, the third storey is added as one of the possible damage locations. The correct damage hypothesis is extended one more step and bounded for further branching because the posterior probabilities of the extended hypotheses are lower than that of the correct hypothesis.

Figure 4 follows a depth-first/best-first search strategy. After the first extension of H[0] to H[1], H[4], H[6], H[5], H[2] and H[3], $P(\text{H}[6]|\hat{\Psi}_{N_s})$ is assigned to $P^3_{\max}$. Since the posterior probabilities of H[1], H[4] and H[6] are larger or equal to the current $P^3_{\max}$, only these three branches remain for further extensions. Next, H[1]

Table III. Effect of damage amount

Case	Damage amount: Second storey	Damage amount: Sixth storey	Rank
1	30%	10%	1
2	60%	20%	21
3	90%	30%	28

DOFm $= \{2, 4\}$, $N_s = 5$, MODEm $= \{1, 2\}$, noise $= 5\%$

is extended since H[1] has the highest posterior probability among H[1], H[4] and H[6] (best-first search). After this extension, $P^3_{\max}$ is changed to $P(\mathrm{H}[1,4]|\hat{\Psi}_{N_s})$. Among the subtrees of H[1], only H[1, 6], H[1, 5] and H[1, 4] remain for further extensions. In the next step, since we employ a depth-first search scheme, H[1, 6] is first extended rather than H[4]. When we extend H[4] to H[4, 6], H[4, 5], H[2, 4] and H[3, 4], all branches below H[1] are already extended. That is, at this stage, $P^3_{\max}$ has been changed to $P(\mathrm{H}[1,2,5,6]|\hat{\Psi}_{N_s})$ which is the third largest posterior probability among the hypotheses examined so far. Since the posterior probabilities of H[4, 6], H[4, 5], H[2, 4] and H[3, 4] are less than the current $P^3_{\max}$, further extensions are excluded.

In place of the largest posterior probability in equation (27), Figure 4 uses the third largest posterior probability among the hypotheses examined so far as the pruning criterion. If the largest posterior probability had been used in Figure 4, the branching from hypothesis H(1) to H(1, 5) would have been excluded. For the detection of multiple damage locations, the pruning heuristic in the branch-and-bound search scheme should be loosened to include a larger subspace of the hypothesis space. Examining more hypotheses increases the chance of capturing the actual damage event. In real situations, the proposed method may not find *all* the damaged substructures, but, very likely it can find the damage locations which have *significant* effect on the modal parameters.

3.1.4. Effect of damage amount. For all three cases in Table III, we assume a 5 per cent noise level, five sets of modal data, and the estimation of the first and the second modes with the measurement on the second and the fourth storeys. The proposed method identifies the actual damage event for case 1, where 30 and 10 per cent decreases in the stiffness are simulated in the second and the sixth storeys, respectively. As damage in the second and the sixth storeys, respectively, increases to 60 and 20 per cent (case 2), the rank of the actual damage event decreases. When more severe damage is assumed for case 3 ($\hat{L}_{\mathrm{dam}} = \{2, 6\}$ and $\hat{D}_{\mathrm{dam}} = \{90\%, 30\%\}$), the rank of the actual damage event becomes lower. In spite of the absolute increase of damage in both the storeys from case 1 to cases 2 and 3, the diagnosis result worsens. This phenomenon can be explained as follows: Since, in the current example structure, the second-storey stiffness has more significant effect on the modal parameters and larger damage than the sixth-storey stiffness, the second storey becomes more detectable than the sixth storey (for all cases, the branch-and-bound search identifies the second storey first). On the other hand, the sixth storey becomes less detectable as the difference of damage between the second and the sixth storeys increases. This implies that, for the detection of multiple damage locations, the proposed method depends on the *relative* damage amount among the damaged substructures as well as the *absolute* damage amount of each substructure.

The cases shown in Table III use a value of 0.9 as the damage threshold value θ^* for all substructures. That is, the damaged substructures with less than 10 per cent stiffness decrease may not be detected. If a higher damage threshold value (> 0.9) and a smaller $\Delta\theta$, which is an incremental value implemented to search the non-dimensional parameter space $\Theta_{\mathrm{H}_j} < \Theta^*_{\mathrm{H}_j}$ in equation (7), are used, the proposed method can identify smaller damage. For the cases shown in Table IV, we set the damage threshold value θ^* to 0·99 and the incremental value $\Delta\theta$ to 0·01. Four cases are conducted by changing the damage locations and amount. For all cases, less than 10 per cent stiffness decrease is assumed. In spite of a small damage amount, all cases

Table IV. Detection of small damage

Case	L_{dam}	D_{dam}	Noise	N_s	Rank
1	{3}	{3%}	2%	20	1
2	{1, 3}	{5%, 5%}	2%	100	1
3	{2, 6}	{5%, 3%}	5%	100	1
4	{2, 3}	{5%, 3%}	5%	50	1

DOFm = {2, 4}, MODEm = {1, 2}

Table V. Effect of mode selection

Case	Estimated modes	Rank
1	all	1
2	1, 2	8
3	3, 4	1
4	5, 6	7

$L_{dam} = \{2, 6\}$, $D_{dam} = \{30\%, 10\%\}$, $N_s = 3$, DOFm = {2, 4}, noise = 5%

converge to the actual damage event. The problem is that the smaller the incremental value $\Delta\theta$, the more the computation time is required. Also the measured data with lower noise level is necessary for the detection of small damage.

3.1.5. Effect of mode selection. To study the effect of mode selection, the estimated modes are changed for each case. For all cases, the damage amount of the second and the sixth storeys is assumed to be 30 and 10 per cent, respectively. Three modal data sets are collected and a 5 per cent noise level is assumed. Measurements are made on the second and the fourth storeys.

Table V presents the diagnosis results obtained by using four different mode selection strategies. When all six modes are estimated in case 1, the proposed method ranks the actual damage event as the most probable one. From the results of cases 2–4, where two different modes are estimated for each case, it appears that the selection of the third and the fourth modes yields better assessment than the other two selection strategies for the detection of the assumed damage locations $L_{dam} = \{2, 6\}$.

What modes should be selected depends on the specified damage locations. Unfortunately, for the damage detection of civil structures, selecting specific modes may not be practical because (1) usually only a few fundamental modes can be estimated from the vibration test of a structure, and (2) the contribution of a mode for the damage detection depends on the actual damage locations which are unknown when modes are selected.

3.1.6. Effect of the number of modal data sets. Better damage assessment can be achieved by accumulating modal data sets from vibration tests. To investigate the effect of the number of modal data sets N_s, four cases are conducted by increasing N_s from 1 to 10. For all cases, $L_{dam} = \{2, 6\}$, $D_{dam} = \{30\%, 10\%\}$ and a 5 per cent noise level are assumed. The first and the second modes are estimated by the measurements on the second and the fourth storeys. The diagnosis results presented in Table VI show that the proposed method identifies the actual damage locations when $N_s \geqslant 5$. For case 1, since the branch-and-bound search does not find the actual damage event, the rank of the actual damage event is denoted as *not found* in Table VI.

Table VII shows the results of the re-diagnosis of the previous cases, which failed to rank the actual damage event as the most probable one, by increasing the number of data sets. For the previous case 3 of Table I, the rank of the actual damage event changes from eighth to first after increasing the number of data sets N_s

Table VI. Effect of data set number

Case	N_s	Rank
1	1	not found
2	3	8
3	5	1
4	10	1

$L_{dam} = \{2, 6\}, D_{dam} = \{30\%, 10\%\}$, noise = 5%, DOFm = {2, 4}, MODEm = {1, 2}

Table VII. Improvement of diagnosis results by increasing data set number

Case	D_{dam}	Noise	MODEm	DOFm	N_s	Rank
Case 2 of Table I	{30%, 10%}	1%	{1, 2}	{2, 4}	3→5	5→1
Case 3 of Table I	{30%, 10%}	5%	{1, 2}	{2, 4}	3→5	8→1
Case 4 of Table I	{30%, 10%}	10%	{1, 2}	{2, 4}	3→20	10→1
Case 2 of Table III	{60%, 20%}	5%	{1, 2}	{2, 4}	5→10	21→1
Case 3 of Table III	{90%, 30%}	5%	{1, 2}	{2, 4}	5→10	28→1
Case 4 of Table V	{30%, 10%}	5%	{5, 6}	{2, 4}	3→20	7→1
Case 3 of Table II	{30%, 10%}	10%	{1, 2}	{3, 5}	5→20	15→1
Case 4 of Table II	{30%, 10%}	10%	{1, 2}	{2, 4}	5→20	14→1
Case 5 of Table II	{30%, 10%}	10%	{1, 2}	{3}	5→20	13→9

For all cases, $L_{dam} = \{2, 6\}$

from 3 to 5. Table VII also shows the other cases in which the actual damage locations are properly detected after increasing N_s. However, for the previous case 5 of Table II, where only one DOF is measured, the proposed method fails to identify the actual damage locations even after increasing N_s to 20. This illustrates that sufficient measured DOFs and number of data sets are required for damage detection.

3.2. A two-storey three-dimensional frame structure

A two-storey frame structure, shown in Figure 5, is employed to validate the proposed method for three-dimensional problems. The analytical model is assumed to be identical to the actual structure, and has 48 DOFs (24 rotational DOFs and 24 translational DOFs). Each beam and column is modelled as a substructure. Altogether, the system consists of 16 substructures. For all the cases considered in this example, five fundamental modes are estimated. The modal parameters are measured at 5 DOFs out of the total 48 DOFs. Two configurations of the measured DOFs are shown in Figure 6. In addition, three sets of the estimated modal parameters are simulated by perturbing the exact modal parameters with a 5 per cent noise level.

As shown in Table VIII, the four cases are conducted by changing the damage locations and amount. The modal parameters are measured at the DOFs shown in Figure 6(a). For case 1, the first substructure is subject to a 20 per cent decrease in the stiffness. Case 2 assumes 20 and 40 per cent stiffness decreases in the 10th and the 11th substructures, respectively. Case 3 assumes 20 and 40 per cent stiffness decreases in the 1st and the 14th substructures, respectively. All the damaged substructures are shown as circled numbers in Figure 5. For cases 1 and 2, the proposed method finds the exact damage locations as well as the exact damage amount. Case 3 ranks the actual damage event as the second most probable event; the most probable event corresponds to the actual damage locations (the 1st and the 14th substructures) with one extra location (the 11th substructure). After increasing the number of modal data sets from 5 to 10, the actual damage event is properly identified as the most likely one as shown in case 4.

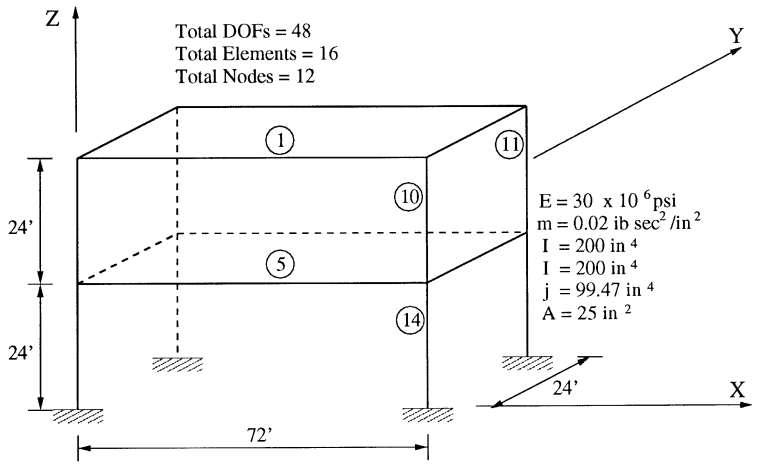

Figure 5. A two-storey frame structure

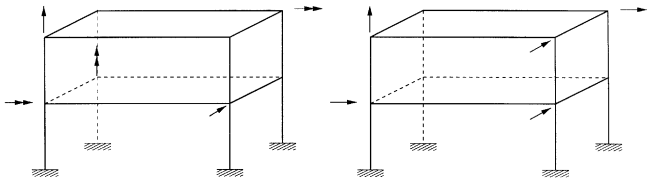

Figure 6. Two different configurations of measured DOFs

Table VIII. Diagnosis results of a two-storey frame structure

Case	Actual damage L_{dam}	Actual damage D_{dam}	Estimated damage $\hat{L}_{dam}$	Estimated damage $\hat{D}_{dam}$	N_s	Rank
1	{1}	{20%}	{1}	{20%}	5	1
2	{10, 11}	{20%, 40%}	{10, 11}	{20%, 40%}	5	1
3	{1, 14}	{20%, 40%}	{1, 11, 14}	{20%, 20%, 40%}	5	1
			{1, 14}	{20%, 40%}		2
4	{1, 14}	{20%, 40%}	{1, 14}	{20%, 40%}	10	1

DOFm = {3, 16, 28, 32, 48}, MODEm = {1, 2, 3, 4, 5}, noise = 2%, $N_s = 5$

Table IX investigates the effect of measured DOFs on damage detection by comparing two different configurations of measured DOFs as shown in Figure 6. 20 and 40 per cent damage are assumed in the first and the fifth substructures for both cases. Since the actual damage event is not found by the branch-and-bound search for case 5, the rank of the actual damage event is represented as *not found* in Table IX. In dynamic analyses, the inertial effects associated with rotational DOFs are usually small. In addition, the axial deformations of beams and columns can be ignored in many cases. As a result, lateral DOFs provide more information than rotational and vertical DOFs. For case 5, three rotational, one vertical and one horizontal

Table IX. Comparison of two measurement strategies

Case	DOFm	Rank
5	$\{3, 16, 28, 32, 48\}$	not found
6	$\{8, 13, 20, 25, 32\}$	1

MODEm $= \{1, 2, 3, 4, 5\}$, noise $= 2\%$, $N_s = 5$, $L_{dam} = \{1, 5\}$, $D_{dam} = \{20\%, 40\%\}$

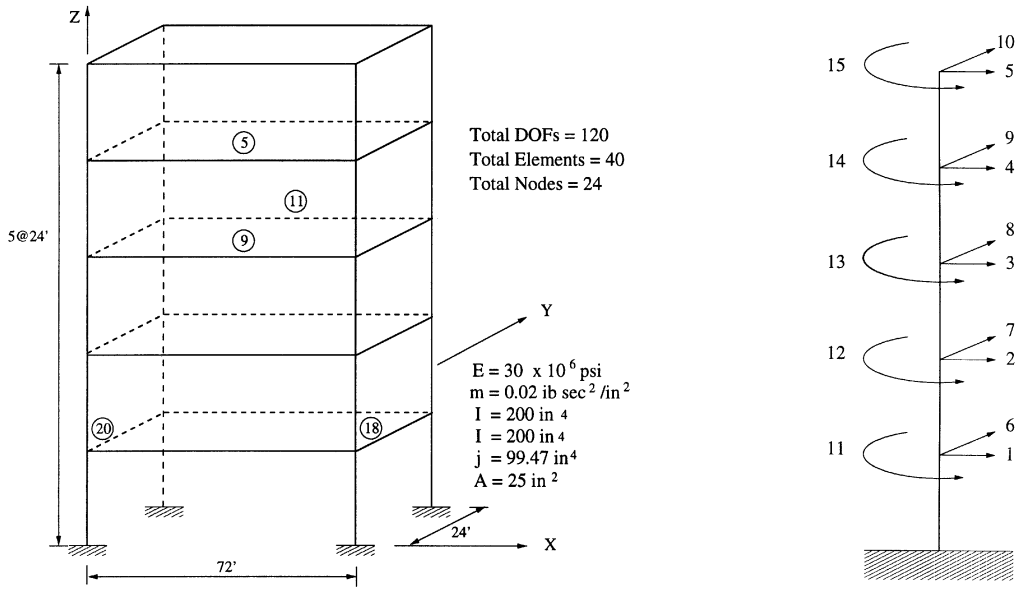

Figure 7. The baseline structure and the simplified model of a five-storey frame structure

DOFs (DOFm $= \{3, 16, 28, 32, 48\}$) are measured, and for case 6 the measured DOFs {8, 13, 20, 25, 32} are all lateral DOFs. The results of Table IX show that the measured DOFs in case 6 are more appropriate for the detection of damage in the first and the fifth substructures.

3.3. A five-storey three-dimensional frame structure

The applicability of the proposed method is illustrated when differences exist between the baseline structure and the simplified model. The first example neglects the measurement noise to highlight the effect of modelling error, and the second example considers both modelling and noise errors. In this example, a FE model of a five-storey frame structure serves as the baseline structure. The term *baseline structure* is used to represent a structure from which the experimental modal parameters are simulated. A simplified model, which the proposed method works with, is formed by employing the modelling approach described in Section 2.4. Furthermore, for the calculation of $e_M(\Theta_{H_0})$ in equation (18), $\hat{\psi}_m^h$ is simulated by perturbing the modal parameters of the initial FE model with noise. $\psi(\Theta_{H_0})$ is obtained by solving an eigenvalue problem of the simplified model. That is, $e_M(\Theta_{H_0})$ is defined as the modal error caused by the difference between the baseline structure and the simplified model.

Figure 7(a) and 7(b) show the baseline structure and the simplified model, respectively. While the baseline structure has six DOFs at each node (three translational and three rotational DOFs), the simplified model has

Table X. Effect of modelling error in a five-storey frame structure

Case	Actual damage L_{dam}	Actual damage D_{dam}	Estimated damage $\hat{L}_{\text{dam}}$	Estimated damage $\hat{D}_{\text{dam}}$	N_s
1	{5,9}	{50%,50%}	{5,9}	{60%,50%}	1
2	{9,11}	{40%,60%}	{9,11}	{50%,70%}	1
3	{18,20}	{20%,10%}	{18,20}	{20%,10%}	1

Noise = 0%, DOFm = $\{1, 2, \ldots, 15\}$, MODEm = $\{1, 2, \ldots, 6\}$

only three DOFs at the mass centre of each floor. For the current five-storey example, the baseline structure has 120 DOFs and the simplified model has 15 DOFs. In many vibration tests of building structures, modal vectors are evaluated at the mass centre of the floor diaphragm. To simulate the estimated modal vectors of a structure, the modal vector of the FE model is reconstructed at the mass centre of every floor. That is, the components of the estimated modal vector correspond with those of the simplified model. The first six fundamental modes are assumed to be estimated. The first and fourth modes are the first and second bending modes, respectively, in the X-direction of Figure 7. The second and fifth modes are the first and second bending modes, respectively, in the Y-direction. Furthermore, the third and sixth modes correspond to the first and second torsional modes, respectively.

3.3.1. Consideration of modelling error. Table X shows the diagnosis results of three different damage scenarios, considering the difference between the baseline structure and the simplified model. Case 1 assumes a 50 per cent stiffness decrease in the fifth and the ninth substructures. For case 2, 40 and 60 per cent decreases in the stiffness are imposed on the 9th and the 11th substructures, respectively. Case 3 assumes 20 and 10 per cent stiffness decreases in the 18th and the 20th substructures, respectively. Figure 7(a) shows the damaged substructures as circled numbers. Beams and columns in the baseline structure are defined as substructures. Since the stiffness matrix of the simplified system is represented as an assembly of the effective stiffness contribution of each substructure [see equation (34)], damage locations can be tracked at the substructure level of the baseline structure. That is, damage locations are identified in the baseline structure, not in the simplified model.

For all cases, the proposed method properly identifies the actual damage locations. The estimated damage amount is, however, slightly different from the actual damage amount for cases 1 and 2. This can be explained as follows: We search for the most likely hypothesis $\mathrm{H}_{\max}$ and the corresponding non-dimensional parameter value $\Theta_{\mathrm{H}_{\max}}^{\max}$ which minimize the approximated error function $J(\hat{\Psi}_{N_s}, \Theta_{\mathrm{H}_j})$ defined in equation (22). For the exact definition of $J(\hat{\Psi}_{N_s}, \Theta_{\mathrm{H}_j})$, $e_{\mathrm{M}}(\Theta_{\mathrm{H}_d})$, which is the modal error caused by the modelling error after damage occurrence, should be evaluated. However, the actual damage locations and amount, which are required to evaluate $e_{\mathrm{M}}(\Theta_{\mathrm{H}_d})$, are unknown. Therefore, $e_{\mathrm{M}}(\Theta_{\mathrm{H}_d})$ is approximated by $e_{\mathrm{M}}(\Theta_{\mathrm{H}_0})$, which is the modal error caused by the modelling error before damage occurrence, assuming that the modelling error is constant for arbitrary damage locations and amount ($e_{\mathrm{M}}(\Theta_{\mathrm{H}_j}) \cong e_{\mathrm{M}}(\Theta_{\mathrm{H}_0})$; $\forall \Theta_{\mathrm{H}_j}$).

For comparison of $e_{\mathrm{M}}(\Theta_{\mathrm{H}_0})$ and $e_{\mathrm{M}}(\Theta_{\mathrm{H}_j})$, the selected components of $e_{\mathrm{M}}(\Theta_{\mathrm{H}_0})$ and $e_{\mathrm{M}}(\Theta_{\mathrm{H}_j})$ are listed in Table XI. The error components corresponding to the first six frequencies are shown in part (a) of Table XI. Next the error components corresponding to the measured modal vectors are presented in part (b). For simplicity, only the components corresponding to the DOFs 1–5 are tabulated for the first and fourth modal vectors (the first two bending modes along the X-direction). Similarly, the components corresponding to the DOFs 6–10 are presented for the second and fifth modal vectors (the first two bending modes along the Y-direction), and the components corresponding to the DOFs 11–15 are presented for the third and sixth modal vectors (the first two torsional modes). $e_{\mathrm{M}}(\Theta_{\mathrm{H}_j})$ is computed for the three damage cases in Table X. To provide a relative measure on the magnitude of $e_{\mathrm{M}}(\Theta_{\mathrm{H}_0})$, the components of $\psi(\Theta_{\mathrm{H}_0})$ corresponding to

Table XI. Comparison of $e_M(\Theta_{H_0})$ and $e_M(\Theta_{H_j})$

	$\psi_i(\Theta_{H_0})$	$e_{M,i}(\Theta_{H_0})$	$e_{M,i}(\Theta_{H_j})$ Case 1	Case 2	Case 3
		(a) Components corresponding to the frequencies			
Mode	ω_i				
1	1·7313	0·0030	0·0053 (0·13%)	0·0035 (0·02%)	0·0030 (0·00%)
2	2·4566	0·0281	0·0282 (0·00%)	0·0282 (0·00%)	0·0281 (0·00%)
3	2·9106	0·0070	0·0079 (0·03%)	0·0082 (0·04%)	0·0076 (0·02%)
4	5·7511	0·0157	0·0014 (0·30%)	0·0078 (0·14%)	0·0157 (0·00%)
5	7·6658	0·0935	0·0943 (0·01%)	0·0948 (0·02%)	0·0948 (0·02%)
6	9·1053	0·0956	0·0557 (0·44%)	0·0415 (0·59%)	0·0981 (0·03%)
		(b) Components corresponding to the modal vectors			
DOF	$\mathbf{v}_1$				
1	0·1559	0·0003	0·0002 (0·06%)	0·0002 (0·05%)	0·0003 (0·00%)
2	0·4274	0·0009	0·0004 (0·12%)	0·0006 (0·05%)	0·0009 (0·00%)
3	0·6865	0·0013	0·0001 (0·17%)	0·0011 (0·03%)	0·0013 (0·00%)
4	0·8822	0·0012	0·0007 (0·06%)	0·0011 (0·02%)	0·0012 (0·00%)
5	1·0000	0·0000	0·0000 (0·00%)	0·0000 (0·00%)	0·0000 (0·00%)
DOF	$\mathbf{v}_2$				
6	0·1998	0·0014	0·0014 (0·00%)	0·0014 (0·00%)	0·0015 (0·03%)
7	0·4834	0·0029	0·0029 (0·00%)	0·0029 (0·00%)	0·0031 (0·02%)
8	0·7312	0·0032	0·0032 (0·00%)	0·0032 (0·00%)	0·0033 (0·01%)
9	0·9077	0·0018	0·0018 (0·00%)	0·0018 (0·00%)	0·0019 (0·01%)
10	1·0000	0·0000	0·0000 (0·00%)	0·0000 (0·00%)	0·0000 (0·00%)
DOF	$\mathbf{v}_3$				
11	0·1987	0·0001	0·0002 (0·03%)	0·0002 (0·02%)	0·0002 (0·05%)
12	0·4849	0·0022	0·0019 (0·07%)	0·0018 (0·08%)	0·0020 (0·04%)
13	0·7345	0·0029	0·0027 (0·02%)	0·0031 (0·04%)	0·0029 (0·01%)
14	0·9102	0·0013	0·0016 (0·03%)	0·0019 (0·06%)	0·0014 (0·01%)
15	1·0000	0·0000	0·0000 (0·00%)	0·0000 (0·00%)	0·0000 (0·00%)
DOF	$\mathbf{v}_4$				
1	0·4996	0·0005	0·0006 (0·04%)	0·0005 (0·01%)	0·0005 (0·00%)
2	0·9619	0·0022	0·0011 (0·11%)	0·0002 (0·21%)	0·0022 (0·00%)
3	0·6984	0·0084	0·0059 (0·36%)	0·0071 (0·19%)	0·0084 (0·00%)
4	−0·1532	0·0119	0·0103 (1·05%)	0·0119 (0·01%)	0·0119 (0·00%)
5	−1·0000	0·0000	0·0000 (0·00%)	0·0000 (0·00%)	0·0000 (0·00%)
DOF	$\mathbf{v}_5$				
6	0·5963	0·0004	0·0003 (0·01%)	0·0003 (0·01%)	0·0013 (0·15%)
7	1·0000	0·0000	0·0000 (0·00%)	0·0000 (0·00%)	0·0000 (0·00%)
8	0·6238	0·0017	0·0016 (0·02%)	0·0016 (0·02%)	0·0024 (0·11%)
9	−0·2603	0·0020	0·0022 (0·06%)	0·0025 (0·18%)	0·0025 (0·17%)
10	−0·9869	0·0071	0·0069 (0·03%)	0·0062 (0·10%)	0·0070 (0·09%)
DOF	$\mathbf{v}_6$				
11	0·5824	0·0021	0·0180 (2.73%)	0·0319 (5.12%)	0·0038 (0·29%)
12	0·9756	0·0053	0·0447 (4·04%)	0·0748 (7.12%)	0·0015 (0·39%)
13	0·5881	0·0125	0·0529 (6.86%)	0·0855 (12.4%)	0·0095 (0·51%)
14	−0·2931	0·0164	0·0348 (6.30%)	0·0466 (10·3%)	0·0148 (0·54%)
15	−1·0000	0·0000	0·0000 (0·00%)	0·0000 (0·00%)	0·0000 (0·00%)

* The value in ( ) represents the normalized error, $100 \times |e_{M,i}(\Theta_{H_0}) - e_{M,i}(\Theta_{H_j})|/\psi_i(\Theta_{H_0})$, in percentage

Table XII. Effect of modelling and noise errors in a five-storey frame structure

Case	Actual damage L_{dam}	Actual damage D_{dam}	Estimated damage $\hat{L}_{\text{dam}}$	Estimated damage $\hat{D}_{\text{dam}}$	N_s
1	{5,9}	{50%,50%}	{5,9}	{60%,50%}	5
2	{9,11}	{40%,60%}	{9,11}	{50%,70%}	10
3	{18,20}	{20%,10%}	{18,20}	{20%,10%}	10

Noise = 5%, DOFm = $\{1, 2, \ldots, 15\}$, MODEm = $\{1, 2, \ldots, 6\}$

those of $e_M(\Theta_{H_0})$ are presented in the first column of each table. Furthermore, a normalized error defined as $100 \times |e_{M,i}(\Theta_{H_0}) - e_{M,i}(\Theta_{H_j})|/\psi_i(\Theta_{H_0})$ is parenthesized next to each $e_{M,i}(\Theta_{H_j})$ value.

For cases 1 and 2 of Table XI, larger differences between $e_M(\Theta_{H_j})$ and $e_M(\Theta_{H_0})$ than those of case 3 are observed especially in the components corresponding to mode 6. This explains why the estimated damage amount is slightly different from the actual damage amount for cases 1 and 2. It appears that $|e_{M,i}(\Theta_{H_0}) - e_{M,i}(\Theta_{H_j})|$ increases for higher modes. However, the magnitude of $|e_{M,i}(\Theta_{H_0}) - e_{M,i}(\Theta_{H_j})|$ remains less than 1 per cent of the corresponding $\psi_i(\Theta_{H_0})$ for most components. Since the damage amount is small in case 3, the change of the modelling error is negligible, and the proposed method identifies the exact damage amount as well as the correct damage locations. From this simplification, we are able to reduce the size of the system from 120 DOFs to 15 DOFs without losing significant accuracy.

3.3.2. Consideration of modelling and noise errors. Finally, the measurement noise and the modelling error are taken into account together to validate the robustness of the proposed method. The same damage scenarios in Table X are re-investigated. The only difference from the previous cases is that the modal parameters of the FE model are corrupted with 5 per cent noise. Table XII summarizes the diagnosis results. After increasing the number of modal data sets to a certain number, the proposed method identifies the actual damage locations even in the presence of the measurement noise and the discrepancy between the baseline structure and the simplified model.

4. CONCLUSIONS AND DISCUSSION

In this paper, a Bayesian probabilistic approach has been applied to detect the most likely locations and amount of damage in a structure. The system stiffness matrix is represented as an assembly of the substructure stiffness matrices and a non-dimensional parameter θ_i is introduced to model the stiffness contribution of the ith substructure. The mass matrix is assumed to be known and invariant. Assuming a uniform probability density function for the non-dimensional parameter θ_i ($0 \leqslant \theta_i \leqslant 1$), we formulate the relative posterior probability of an assumed damage event and apply a branch-and-bound search scheme to identify the most likely damage event. The measurement noise and modelling error between the structure and the analytical model are explicitly considered within the Bayesian probabilistic framework.

Several examples using a shear frame structure, a two-storey and a five-storey three-dimensional frame structure are simulated to assess the potential applicability of the proposed method. As long as sufficient modal data sets are available, the proposed method is able to identify the actual damage locations and amount in most cases where (1) less than 10 per cent noise levels are achieved in the estimated modal parameters, (2) only 10–30 per cent out of the total degrees of freedom are measured, and (3) only several fundamental modes are estimated. The computational cost of the method is significantly reduced by using a branch-and-bound search scheme.

While this paper has illustrated the potential applicability of the Bayesian probabilistic approach to damage detection, many interesting research issues remain. First, the computational effort to find the most likely non-dimensional parameter value $\Theta_{\mathrm{H}_j}^{\max}$ in equation (7), increases exponentially with the number of potentially damaged substructures included in the hypothesis H_j. The computation could become prohibitive when $\Theta_{\mathrm{H}_j}^{\max}$ is calculated for a hypothesis H_j which assumes a large number of substructures as damaged. Further effort is required to develop an efficient method to evaluate $\Theta_{\mathrm{H}_j}^{\max}$.

Second, damage detection techniques, which rely only on the modal parameter information such as the one described in this paper, might have the drawback that the damage locations and amount may not be uniquely determined from the estimated modal data.[25] Models with differently assumed damage locations and amount can produce identical modal parameters. These models are referred to as *output-equivalent* models.[5] The exhaustive search of all possible models (hypotheses) is infeasible, and a branch-and-bound search scheme may identify only some models (hypotheses with assumed damage locations and amount), which locally maximize the posterior probability $P(\mathrm{H}_j|\hat{\Psi}_{N_s})$ in equation (5), and may not detect the global maximum points. In real applications, (1) since the modal testing measures the dynamic responses at limited points and estimates only a few fundamental modes, the number of output-equivalent models can increase, and (2) in the presence of the modelling error and the measurement noise, some erroneous models could have modal parameters closer to the estimated modal parameters than the model with the correct damage locations and amount. Therefore, in practice, more hypotheses should be examined to find more local maximum posterior probabilities and potentially to identify the correct damage event. In the proposed method, a larger subspace of the hypothesis space can be examined by replacing $P_{\max}$ in equation (27) with $P_{\max}^n$, where $P_{\max}^n$ is the nth largest posterior probability among the hypotheses examined so far. This approach allows us to make an explicit trade-off between the computational cost and the better diagnosis. However further research is required to provide a systematic guideline for choosing 'n' in $P_{\max}^n$.

Third, damage is simulated as the deterioration of substructure or element stiffnesses in this paper. In real structures, damages are developed in the form of fatigue cracks, loose connections, local bucklings and so on. It is not clear if the substructure approach can capture these kinds of real damage within the substructure. Further study is required to relate the physical damage phenomena to the mathematical damage models.

The proposed method is superior to the deterministic approaches, which produce a single diagnosis result, in that (1) several suspicious damage events are provided with their relative possibilities, (2) a series of measurement data obtained from vibration tests can be included to improve the accuracy of the results, and (3) engineering judgment about possible damage events via some system reliability analysis or experience with similar structures can potentially be incorporated into the Bayesian framework as the prior probabilities of the damage events.

ACKNOWLEDGEMENTS

This research is partially sponsored by the National Science Foundations under Grant No. CMS-95261-2. Valuable discussions with Professor Anne S. Kiremidjian and Mr. Erik G. Straser at Stanford University and Professor James L. Beck at California Institute of Technology are sincerely appreciated. The comments by the reviewers are also appreciated.

REFERENCES

1. G. H. James, D. C. Zimmerman, C. R. Farrar, S. W. Doebling, 'Current horizon for structural damage detection course', *SEM short course held at the 15th Int. Modal Analysis Conf.*, Orlando, FL, 1997.
2. S. W. Smith and C. A. Beattie, 'Secant-method adjustment for structural models', *AIAA* **29**, 119–126 (1991).
3. D. C. Kammer, 'Optimum approximation for residual stiffness in linear system identification', *AIAA* **26**, 104–112 (1988).
4. A. M. Kabe, 'Stiffness matrix adjustment using mode data', *AIAA* **23**, 1431–1436 (1985).
5. L. S. Katafygiotis, 'Treatment of model uncertainties in structural dynamics', *EERL Report No. 91-01*, Earthquake Engineering Research Laboratory, California Institute of Technology, Pasadena, CA, 1991.
6. D. C. Zimmerman and M. Kaouk, 'Structural damage detection using a subspace rotation algorithm', *Proc. 33rd AIAA/ASME/ASCE/AHS Structure, Structural Dynamics and Materials Conf.*, Dallas, TEX, 1992.

7. M. Kaouk and D. C. Zimmerman, 'Structural damage assessment using a generalized minimum rank perturbation theory', *Proc. 34th AIAA/ASME/ASCE/AHS Structure, Structural Dynamics and Material Conf.*, La Jolla, CA, 1993.
8. J. L. Beck, M. W. Vanik and L. S. Katafygiotis, 'Determination of stiffness changes from modal parameter changes for structural health monitoring', *Proc. 1st World Conf. on Structural Control*, Pasadena, CA, 1994.
9. F. M. Hemez, 'Theoretical and experimental correlation between finite element models and modal tests in the context of large flexible space structures', *Ph.D. Thesis*, Department of Aerospace Engineering, University of Colorado at Boulder, Boulder, COL, 1993.
10. J. M. Ricles and J. B. Kosmatka, 'Damage detection in elastic structures using vibratory residual forces and weighted sensitivity', *AIAA* **30**, 2310–2316 (1992).
11. S. W. Smith, 'Damage detection and location in large space trusses, *Ph.D. Thesis*, Virginia Polytechnic Institute and State University, Blacksburg, VA, 1988.
12. C. R. Farrar *et al.*, 'Dynamic characterization and damage detection in the I-40 bridge over the Rio Grande', *Report No. LA-12767-MS*, Los Alamos National Laboratory, Los Alamos, NM, 1994.
13. J. S. Bendat and A. G. Piersol, *Random Data*: *Analysis and Measurement procedures*, 2nd edn, Wiley, New York, 1986.
14. E. G. Straser and A. S. Kiremidjian, 'A modular, visual approach to damage monitoring for civil structures', *2nd Int. Workshop on Structural Control*, Hong Kong, 1996.
15. J. L. Beck and L. S. Katafygiotis, 'Probabilistic system identification and health monitoring of structures', *Proc. 10th World Conf. on Earthquake Engineering*, Balkema, Rotterdam, 1992.
16. G. V. Garcia and N. Stubbs, 'Relative performance evaluation of pattern recognition models for nondestructive damage detection (NDD)', *Proc. 15th Int. Modal Analysis Conf.*, Orlando, FL, 1997.
17. J. C. Chen and J. A. Garba, 'On-orbit damage assessment for large space structures', *AIAA* **26**, 1119–1126 (1988).
18. A. Berman and E. J. Nagy, 'Improvements of a large analytical model using test data', *AIAA* **21**, 1168–1173 (1983).
19. J. He and D. J. Ewins, 'Compatibility of measured and predicted vibration modes in model improvement studies', *AIAA* **29**, 798–803 (1991).
20. S. W. Smith and C. A. Beattie, 'Simultaneous expansion and orthogonalization of measured modes for structure identification', *AIAA Report No. 90-1218-CP*, 1990.
21. M. Imregun and D. J. Ewins, 'An investigation into mode shape expansion techniques', *Proc. 11th int. modal analysis conf.*, Kissimmee, FL, 1993.
22. M. Henrion, 'Towards efficient probabilistic diagnosis in multiply connected belief networks', *Influence Diagrams, Belief Nets and Decision Analysis*, Chapter 17, Wiley, Chichester, 1990.
23. A. K. Chopra, *Dynamics of Structures*, Prentice-Hall, Eaglewood Cliffs, NJ, 1995.
24. A. K. Ahmadi, 'Application of system identification in mathematical modelling of buildings', *Ph.D. Thesis*, Department of Civil Engineering, University of Pittsburgh, Pittsburgh, PA, 1986.
25. F. E. Udwadia, D. K. Sharma and P. C. Shah, 'Uniqueness of damping and stiffness distributions in the identification of soil and structural systems', *J. Appl. Mech.* **45**, 180–187 (1978).

